J. Phys. B: At. Mol. Opt. Phys. **42** (2009) 075601 (8pp) doi:10.1088/0953-4075/42/7/075601

Carrier-envelope phase-dependent quantum interferences in multiphoton ionization

Mark J Abel[1,2], Thomas Pfeifer[1,2], Aurélie Jullien[1,2], Phillip M Nagel[1,2], M Justine Bell[1,2], Daniel M Neumark[1,2] and Stephen R Leone[1,2,3]

[1] Departments of Chemistry and Physics, University of California, Berkeley, CA 94720, USA
[2] Chemical Sciences Division, Lawrence Berkeley National Laboratory, Berkeley, CA 94720, USA

E-mail: srl@berkeley.edu

Received 18 September 2008, in final form 19 February 2009
Published 20 March 2009
Online at stacks.iop.org/JPhysB/42/075601

Abstract
The angular distribution of photoelectrons created by multiphoton ionization of xenon atoms by a few-cycle laser pulse shows a carrier-envelope phase (CEP) dependent asymmetry. A simple perturbative model based on a sum over indistinguishable quantum paths describes the observed asymmetry as a function of photoelectron energy and CEP. Although the individual multiphoton transition rates depend on the intensity profile of the pulse, the experimentally measured photoelectron angular distributions are sensitive to the absolute spectral phase of the pulse, including both CEP and chirp. We discuss retrieval of the CEP and chirp from the asymmetry pattern, as well as the potential to extract the scattering phase shift.

(Some figures in this article are in colour only in the electronic version)

1. Introduction

The carrier-envelope phase (CEP) of few-cycle laser pulses is a very important quantity for atomic and molecular physics because of the electric-field response of electrons. The CEP is the temporal offset between the laser cycle maximum and the pulse envelope maximum, converted to a phase ϕ using the laser frequency. Even though the CEP appears in the single-photon dipole transition amplitude in perturbation theory, it does not necessarily affect the transition probability, which is the squared modulus of the amplitude. As a result, CEP effects are not extensively explored. Equally important from an experimental point of view, the frequency comb techniques required to stabilize the CEP [1, 2] were not available until recently. The combination of few-cycle ultrabroadband laser pulses [3], extension of the laser frequency comb all the way to zero frequency [1, 4], and a growing realization that many processes are determined by the laser field and not just the intensity envelope of light pulses have stimulated growing interest in the role of the CEP. Effects of the CEP include the number [5] or wavelength [6] of attosecond light pulses produced in high harmonic generation, the angular distributions of photoelectrons in strong-field tunnelling ionization [7], the localization of electrons in molecular dissociation [8] and the direction of photocurrent in semiconductors [9]. In this paper, we present experimental data showing how the CEP affects the angular distribution of photoelectrons generated at electric field strengths in the multiphoton regime.

Because of the importance of CEP stabilization in the creation of isolated attosecond x-ray pulses by few-cycle driver pulses [5], much effort to date has been focused on the role of the CEP in strong-field processes driven by fields comparable to the Coulomb field that binds valence electrons to atoms and molecules. In this regime, electrons react nearly adiabatically [10, 11] to the oscillating laser field, and processes such as tunnelling [10] and photoemission [12] occur on a sub-cycle (attosecond) timescale. Some work has addressed non-adiabatic dynamics in tunnelling ionization [13, 14], but relatively little research has been directed towards discovering the role of the CEP in the weak-field, perturbative regime, where the laser field is small compared to intra-atomic field strengths. A few experiments have confirmed a role for the

[3] Stephen Leone gratefully acknowledges the generous support of the Morris Belkin Visiting Professorship at the Weizmann Institute of Science.

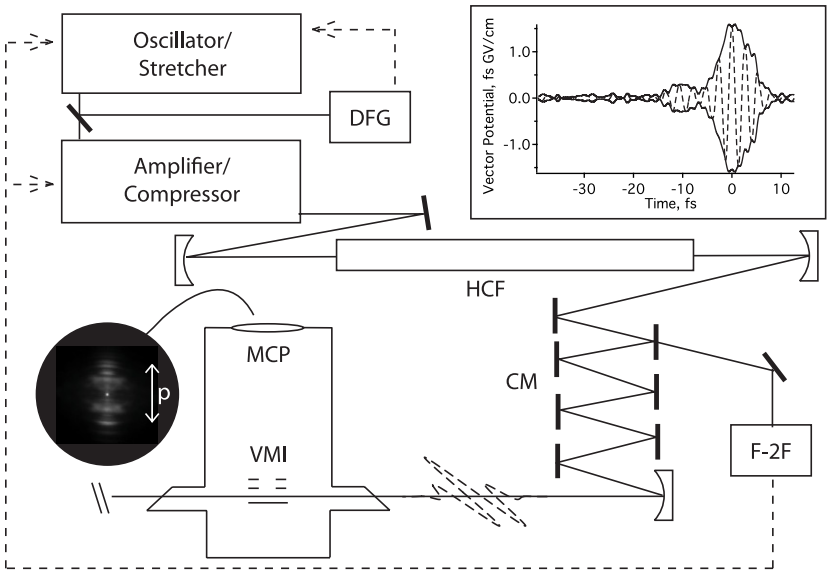

Figure 1. *Experimental setup.* Shown looking down onto the laser table, the polarization direction is out of the plane of the paper. DFG, difference frequency generation and feedback loop for oscillator CEP locking. HCF, hollow-core fibre. CM, chirped mirror compressor. F–2F, f–2f interferometer and feedback loop for amplifier CEP locking. VMI, electrostatic lenses for velocity-map imaging. MCP, multichannel plate electron detector with detector face parallel to the laser polarization direction, *p*. *Inset.* Pulse envelope measured by attosecond streaking in neon (solid line), and an example vector potential to illustrate the relative durations of the carrier wave period and the envelope (dashed line).

CEP in perturbative laser–atom interactions [9, 15, 16] but these works have emphasized CEP stabilization.

Nakajima and Watanabe recently obtained intriguing theoretical results [17] showing a CEP effect in the perturbative regime. They solved the time-dependent Schrödinger equation (TDSE) for caesium atoms exposed to very short perturbative laser fields and found that excited state populations after the laser pulse depend on the CEP; in some cases the populations vary by a factor of 2 or more. Comparing the atom to a 3-level system, they formally solved the perturbation-theoretical differential equations governing the time-dependent state amplitudes. The amplitude for the uppermost state is the sum of four terms, one of which dominates the population in the case of long driving laser pulses. The authors suggested that the CEP effect present in the TDSE results may be due to the other three terms in the overall amplitude, which contribute for very short driving laser pulses.

Recent theoretical work on CEP effects [18] emphasized the role of interferences between distinct multiphoton pathways as the key to understanding CEP effects in both the strong- and weak-field regimes. The multiphoton picture is particularly relevant to the experimental intensity regime here, and we follow the example in [18], interpreting the experimental results in terms of a multiphoton interference picture in which the absolute spectral phase of the laser pulse—CEP and chirp—plays a key role.

Above threshold ionization (ATI) using short laser pulses in the non-perturbative, strong-field regime has been systematically explored by Kling *et al* [19]. This paper focused on high-energy photoelectrons (kinetic energy $\gtrsim$ 10 eV) and did not discuss in detail the asymmetry in the distributions of low-energy photoelectrons. We experimentally visit a lower regime of laser field strength, using 750 nm, 7 fs CEP-stabilized pulses at an intensity of $\sim 3 \times 10^{13}$ W cm^{-2} to photoionize xenon atoms while collecting the full three-dimensional photoelectron momentum distribution, concentrating our analysis on photoelectrons with energies below $\sim$5 eV. When the CE phase ϕ is varied, the angular distribution of photoelectrons changes so that the relative number of photoelectrons going in one direction along the laser polarization versus those going in the opposite direction varies sinusoidally from perfect symmetry. This up–down asymmetry is a function of both the CEP and photoelectron energy and also depends on the chirp of the laser pulse. The asymmetry distribution is interpreted using a simple model that invokes interferences between different quantum pathways leading to the same final photoelectron kinetic energy, resulting from absorption of either N or N+1 photons from opposite ends of the broadband laser spectrum by the atom.

2. Experimental setup

The experiment makes use of a 0.8 mJ, 25 fs, multipass Ti:sapphire amplifier system from FemtoLasers, operating at 3 kHz (figure 1). The output, initially centred at 800 nm wavelength, is spectrally broadened and slightly blue-shifted in a hollow-core fibre filled with 1.7 bar of neon gas before temporal compression using chirped mirrors. The resulting pulse is $\sim$7 fs in duration with 750 nm central wavelength. The compression is adjusted using a pair of fused silica wedges to produce the highest ionization rate in the target gas sample. The strongest ionization, corresponding to the highest peak intensity, is not necessarily coincident with flat spectral phase at the central frequency in the case of current few-cycle pulse generation technology. Therefore, some residual

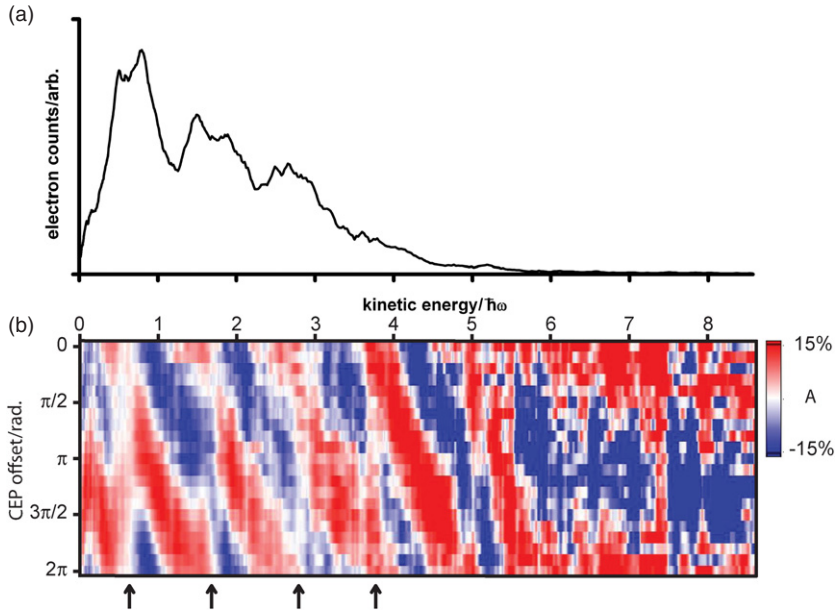

Figure 2. (a) A typical photoelectron momentum spectrum. (b) The up/down asymmetry in the photoelectron spectrum as a function of CEP offset ϕ and electron kinetic energy. Blue fill corresponds to more electrons going upwards in the lab frame (parallel to the laser polarization vector) while red fill corresponds to more electrons going downwards (anti-parallel to the laser polarization vector). The arrows point to kinetic energies where the asymmetry is close to zero independent of CEP. These regions fall at the same kinetic energies as the tops of the peaks in the photoelectron spectrum.

chirp is expected to remain in the pulse at the interaction region. In a separate experiment the temporal profile of the vector potential was measured using attosecond streaking [20] in neon. The individual cycles of the laser pulse were not resolved, but the measured pulse envelope is shown in the inset in figure 1. The streaking data reveal the envelope of the vector potential and indicate that the pulse compression scheme works well, leaving only a small prepulse. The oscillator carrier-envelope offset frequency is detected using difference frequency generation and stabilized using a feedback loop that controls the pump laser output power. Long-term drifts in the CEP of the amplifier are corrected using f–2f interferometry [1] after the hollow-core fibre and a feedback loop that varies both the oscillator pump laser power and the prism insertion in the laser compressor. The CEP jitter of the overall system is measured over a ∼5 s sliding time window by the f–2f interferometer at a spectrometer acquisition rate of ∼30 Hz, with 30 ms exposure time. It ranges from 100 mrad to 300 mrad RMS depending on the day-to-day performance of the amplifier and the spectral broadening.

The photoelectrons generated by multiphoton above-threshold ionization are accelerated towards a two-dimensional position-sensitive detector using velocity map imaging (VMI) [21, 22]. In VMI, all the photoelectrons leaving the interaction region with the same initial velocity vector will be focused to the same spot on the detector, regardless of their initial position. Because of this convenient property of VMI and the cylindrical symmetry of photoemission about the laser polarization axis, the output of the position sensitive detector can be easily inverted to yield the laboratory frame momentum distribution by mathematically taking into account the multiple velocity vectors that can all lead to the same spot on the detector. This is the essence of the basis set expansion (BASEX) [23] method used here.

3. Results

Since we are interested in CEP effects in the multiphoton regime, we reduce the beam diameter and therefore the peak intensity using an adjustable iris aperture to achieve a photoelectron kinetic energy spectrum with only a few peaks and with the first peak the most intense. For above threshold ionization (ATI) with strong laser pulses, the photoelectron kinetic energy corresponding to the maximum intensity in the photoelectron spectrum is roughly equal to the ponderomotive energy U_p [24] of the laser field, and a cutoff exists at $2U_p$ beyond which direct photoemission no longer contributes to the spectrum. Also, the direct photoemission peaks are offset by an amount equal to U_p. The shape of the photoelectron spectrum (figure 2(a)) implies that, in this case, the ponderomotive energy is equal to or less than 1.6 eV, the energy of a single laser photon. Since U_p in eV is equal to $9.33\lambda^2(I/10^{14})$ with λ in microns and I in W cm^{-2}, an upper limit to the intensity is about 3×10^{13} W cm^{-2}. In fact, a ponderomotive shift of 1.6 eV and the ionization potential of Xe (which is 12.1 eV) reproduce the position of the first ATI peak. Since the peak position estimate and the estimate of U_p from the maximum photoelectron intensity agree, they together serve as an estimate for the laser intensity in the interaction region.

Defining the asymmetry $A(\epsilon)$ as the difference in signal between the top and bottom half of the momentum distribution

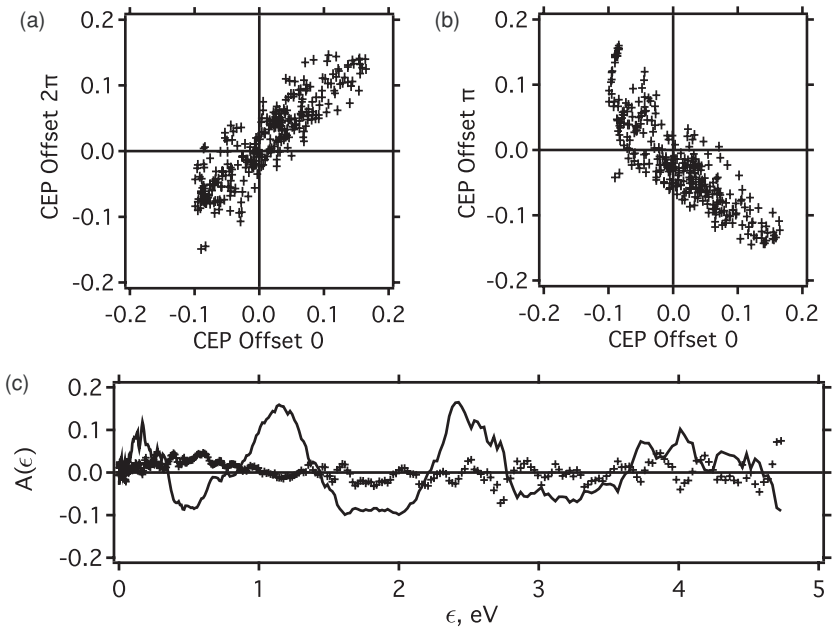

Figure 3. (a) $A(\epsilon)$ for CEP offset set to 2π plotted versus $A(\epsilon)$ for CEP offset set to 0. (b) $A(\epsilon)$ for CEP offset set to π plotted versus $A(\epsilon)$ for CEP offset set to 0. (c) $A(\epsilon)$ for CEP offset 0 (line) and averaged over all CEP values (crosses). The CEP-averaged data would be equivalent to the case of short pulses with no CEP stabilization—the asymmetry is nearly zero for all photoelectron energies.

at a particular photoelectron energy ϵ,

$$A(\epsilon) = \frac{n_{\mathrm{up}}(\epsilon) - n_{\mathrm{down}}(\epsilon)}{n_{\mathrm{up}}(\epsilon) + n_{\mathrm{down}}(\epsilon)}, \tag{1}$$

the result shown in figure 2, panel (b) is obtained. The uppermost asymmetry trace corresponds to an arbitrary and unknown CEP. The CEP is changed by $\pi/10$ for each new measurement, over a total range of 2π. Note that there are certain special photoelectron energies for which the asymmetry is zero regardless of CEP. These energies are spaced by one laser photon energy and correspond to the tops of the peaks in the photoelectron spectrum. They are marked with arrows in figure 2(b). Note also that the pattern between the first and second peaks repeats itself between the second and third peaks, and so on.

Checks are made to ensure that the observed asymmetry is a real effect of the CEP. First, a CEP offset of 2π is equivalent to an offset of 0 so ideally these two asymmetry traces would be perfectly correlated with each other. As shown in panel (a) of figure 3, the correlation between each pair of 0 and 2π points is pronounced when the kinetic energy $\epsilon < 4.6$ eV. The scatter of the data reflects the CEP jitter, which in this experiment was less than 150 mrad, plus the noise accumulated in the data collection and processing. Similarly, because changing the CEP by π corresponds to flipping the laser electric field vertically in the lab frame, one would expect that the asymmetry traces corresponding to any two CEP offsets separated by π radians should be perfectly anticorrelated. This is the case, as illustrated for CEP offset 0 and CEP offset π in panel (b) of figure 3. Finally, when all the asymmetry traces are averaged, corresponding to the case of no CEP stabilization, the resulting asymmetry trace is flat as shown in panel (c) of figure 3.

At intermediate intensities of a few 10^{13} W cm^{-2}, the instantaneous ionization rate is a combination of field-dependent (tunnelling) and intensity-envelope-dependent (multiphoton) ionization, the relative contributions of which can be estimated analytically using the theory of Yudin and Ivanov [13]. The theory is constructed in such a way as to agree with the well-accepted Ammosov–Delone–Krainov (ADK) result in the case of strong fields and to agree with the multiphoton result in the limit of weak fields. Calculating the ionization rate as a function of time for the laser pulse parameters (7 fs duration, $I = 3 \times 10^{13}$ W cm^{-2}) and averaging over the intensity variation in the interaction region indicates that the multiphoton contribution is about half the signal. This is in contrast to the intensity of the short pulses used by Kling *et al* [19] to study CEP effects in the Xe atom, where the multiphoton contribution to the ionization was only about 10%.

4. Multiphoton model

Although the experiment was performed in a regime between pure multiphoton and pure tunnelling ionization, the observed experimental results can be interpreted qualitatively in terms of a multiphoton model based on interference between indistinguishable quantum paths. Amending the model to incorporate tunnelling effects may increase the quantitative agreement, but the essential physics is described by the multiphoton model.

Since the laser pulse has a very large bandwidth, there are multiple combinations of photons, all of different colours, that when ionizing a xenon atom in its ground state would lead to the same continuum kinetic energy for the photoelectron. Each combination of photons carries a characteristic phase, the sum of the spectral phases of the individual frequencies involved.

The relative weights of the different pathways are influenced by the details of the energy level scheme of the particular target atom—for example, pathways with intermediate resonances or near-resonances will be more favourable than non-resonant pathways. All these different pathways add coherently to give the final probability for finding the outgoing electron at a particular outgoing energy and angle. But different combinations of wavelengths do not on their own generate asymmetry along the laser polarization direction in the photoelectron distribution. It requires interference between wavefunctions having different parity, or equivalently, mixing between quantum pathways involving different numbers of photons. Ionization of an odd-parity p-electron in Xe by 8 photons from the blue end of the spectrum will lead to an odd-parity continuum state, while ionization by 9 photons from the red end of the spectrum leads to an even-parity state of the same energy. This is similar to the principle of the f–2f interferometer [1], where the blue region of the laser spectrum interferes with the second harmonic of the red region.

Ignoring interactions with the ion core, the CEP-dependent wavefunction $\Psi(\phi)$ of the outgoing electron can be written as a sum of angular momentum eigenfunctions $Y_{l,m} = P_{l,m}(\theta)\,\mathrm{e}^{\mathrm{i}m\varphi}/\sqrt{2\pi}$ weighted with complex amplitudes $c_{l,m}(\epsilon, \phi)$. Instead of three spatial coordinates, it is convenient to choose the electron energy ϵ and the two angles θ and φ (written together as Ω) as coordinates for Ψ. At any particular value of ϵ quantum pathways with one of two photon numbers are contributing to the photoelectron emission. Grouping the even parity functions with angular momentum quantum numbers (l, m) separately from the odd parity functions with angular momentum quantum numbers (l', m') gives:

$$\Psi(\epsilon, \Omega, \phi) = \sum_{l\,\mathrm{even},m} c_{l,m}(\epsilon, \phi) Y_{l,m}(\Omega) + \sum_{l'\,\mathrm{odd},m'} c_{l',m'}(\epsilon, \phi) Y_{l',m'}(\Omega). \tag{2}$$

The asymmetry as a function of photoelectron energy ϵ and CEP ϕ can be expressed in terms of Ψ; it is the difference between the probability of finding an electron going up and the probability of finding one going down in the lab frame, divided by the total probability of finding a photoelectron at that energy:

$$A(\epsilon, \phi) = \frac{\int_{\mathrm{up}} |\Psi(\epsilon, \Omega, \phi)|^2\,\mathrm{d}\Omega - \int_{\mathrm{down}} |\Psi(\epsilon, \Omega, \phi)|^2\,\mathrm{d}\Omega}{\int_{\mathrm{up}} |\Psi(\epsilon, \Omega, \phi)|^2\,\mathrm{d}\Omega + \int_{\mathrm{down}} |\Psi(\epsilon, \Omega, \phi)|^2\,\mathrm{d}\Omega}. \tag{3}$$

Normalization of Ψ means that the denominator in equation (3) is equal to unity. Inserting Ψ from equation (2) and expanding the sums, the cross terms in each integral cancel unless the functions have non-zero overlap ($m = m'$). Since $m = m'$, the azimuthal contribution to the integrals is simply 2π and the polar integral over pairs of (real-valued) Legendre functions $P_{l,m}$ is all that remains:

$$A(\epsilon, \phi) = 2 \sum_{l,l',m} \{c_{l,m}(\epsilon, \phi) c^*_{l',m}(\epsilon, \phi) + \mathrm{conj.}\} \times \int_0^{\pi/2} \mathrm{d}\theta\, \sin(\theta) P_{l,m}(\theta) P_{l',m}(\theta). \tag{4}$$

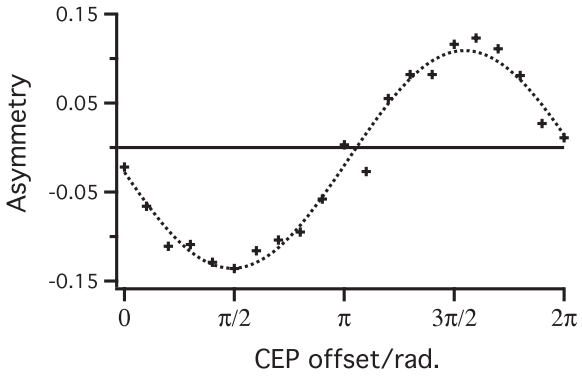

Figure 4. The CEP response of the asymmetry at constant ϵ is sinusoidal in agreement with equation (4). A cut through the experimental data at $\epsilon = 1.6$ eV is marked by the crosses, and the dotted line is a sinusoidal fit to the data.

Each of the amplitude terms contains $\mathrm{e}^{\mathrm{i}\phi} + \mathrm{e}^{-\mathrm{i}\phi}$ and so the asymmetry is cosinusoidal with CEP. We note that the amplitudes c may contain phase contributions other than the CEP; for example, they depend on the laser pulse chirp and on the atomic phase intrinsic to photoionization. These phase contributions may vary with energy, but they do not change the CEP-dependence of the asymmetry at fixed energy.

To simplify equation (4), assume the example of an outgoing wavefunction at a particular energy ϵ_o between the Nth and (N+1)st ATI peaks that is composed of an s-wave (N photons absorbed) and a p-wave (N+1 photons absorbed) with equal weights. The p-wave corresponds to absorption of one extra photon compared to the s-wave, giving it an extra phase contribution equal to the CEP. For this example, also assume that the laser pulse has a perfectly flat spectral phase so there is no chirp, and there are no intrinsic atomic contributions to the phase difference between the two partial waves. Then the only phase difference between the two waves is caused by the extra contribution of the carrier-envelope phase, ϕ, caused by the different number of photons required to reach the even- and odd-parity states. In this case, the wavefunction consists of a sum of two spherical harmonics, separated in phase by the CEP, and each normalized by multiplying by $1/\sqrt{2}$. The wavefunction and asymmetry are

$$\Psi(\epsilon_o, \Omega) = \frac{1}{\sqrt{2}}\left(\frac{1}{\sqrt{4\pi}}\right) + \frac{\mathrm{e}^{\mathrm{i}\phi}}{\sqrt{2}}\left(\frac{\sqrt{3}\cos(\theta)}{\sqrt{4\pi}}\right) \tag{5}$$

$$A(\epsilon_o, \phi) = \left(\frac{\mathrm{e}^{-\mathrm{i}\phi}}{2} + \frac{\mathrm{e}^{\mathrm{i}\phi}}{2}\right) \int_0^{\pi/2} \mathrm{d}\theta \sqrt{3} \sin(\theta)\cos(\theta) \tag{6}$$

$$= \frac{\sqrt{3}}{2}\cos(\phi). \tag{7}$$

The asymmetry in equation (7) varies cosinusoidally with the CEP, which directly matches the experimental observation for CEP variation at fixed energy. Figure 4 shows a cut through the experimental asymmetry plot at a photoelectron kinetic energy of 1.6 eV. The asymmetry does indeed vary as a phase-shifted cosinusoidal function of the CEP offset. This simplified analysis does not take experimental details like spatial averaging of the laser intensity into account. Spatial

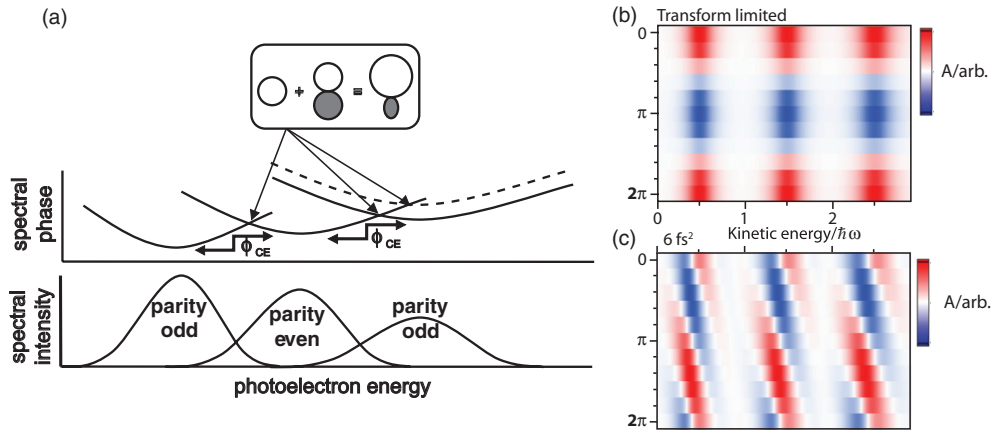

Figure 5. Schematic and simulation of the multiphoton mechanism for CEP effects. (a) The spectral phase of outgoing photoelectron wavepackets of different parity depends on the laser pulse spectral phase. The curves are offset by the CEP, because of the absorption of an additional photon in each case. When the phase difference (mod 2π) vanishes, constructive interference occurs. Tuning the CEP changes the relative offset of the curves, as in the case of the dashed phase curve, and the energies where maximum asymmetry occurs change correspondingly. In this sketch, the photoelectron peaks are drawn wider with increasing energy reflecting the larger spectral width available for excitation with higher numbers of photons. (b) Simulation of the asymmetry as a function of CEP and energy is accomplished by calculating higher order autoconvolutions of the experimental spectrum, assuming flat spectral phase. The asymmetry is then calculated from the amplitudes assuming interference between s waves (even parity states) and p waves (odd parity states). In this case the regions of maximal asymmetry versus CEP are stationary in energy. (c) Adding 6 fs^2 of chirp to the pulse tilts the regions of maximal asymmetry so that they move to higher energy with increasing CEP (adding -6 fs^2 of chirp would make them move to lower kinetic energy).

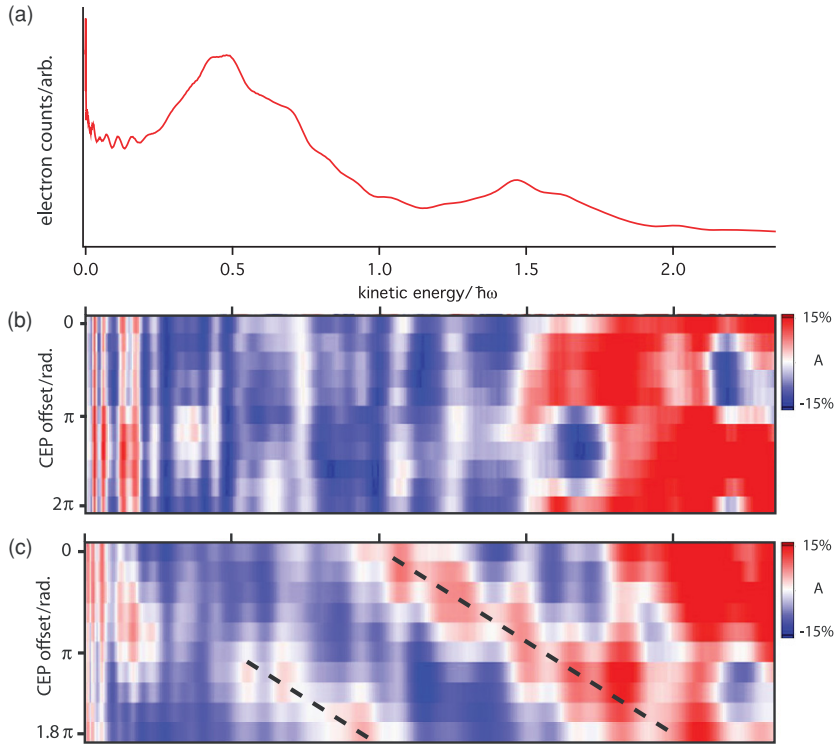

Figure 6. Chirp dependence of the asymmetry. (a) A typical photoelectron spectrum for the chirp-dependence measurements, showing two photoelectron peaks separated by the laser photon energy. (b) When the laser pulse is carefully optimized for flat spectral phase, the regions of maximum asymmetry do not move in energy with varying CEP. (c) After propagation through 160 μm of fused silica, the regions of maximum asymmetry, emphasized by the dotted lines, move with CEP in qualitative agreement with the prediction in figure 5(c).

averaging of the laser intensity in the interaction region does not change the CEP-dependence of the asymmetry, but can affect the yields of photoelectrons into different multiphoton pathways. Thus the spatial averaging does not affect the main conclusions of this paper, namely, that the CEP effects in multiphoton ionization are a result of quantum interferences between different multiphoton pathways.

The current model can be understood as a special case of the work of Roudnev and Esry [18]. It is intended to straightforwardly illuminate the principle of CEP effects

by interference between quantum pathways, with special application to the case of multiphoton ionization of atoms. While it lacks the generality of their work, it describes the experimental data in an illustrative way.

There are other possible contributions to the phases of the partial waves that enter into the angular distribution: specifically, the spectral phase of the laser pulse and an intrinsic atomic phase arising from the (in general multi-electron) interaction between the ion core and the photoelectron after ionization. If the laser pulse is chirped the outgoing photoelectrons will be chirped as well, reflecting the laser pulse that ionizes the atom. However, the chirp of the photoelectron wavepacket for a particular photon number N will not be identical to that of the laser pulse because there are many combinations of N photons, each of different wavelengths, that lead to the same photoelectron energy. The phase contribution due to the chirp, then, is a weighted average of all the possible N-photon pathways, each pathway having its own spectral phase contribution. This is shown schematically in figure 5(a), where the quadratic spectral phase of a linearly chirped laser pulse is mapped onto each outgoing photoelectron wavepacket of alternating parity. The spectral phase curve for each successive photoelectron peak is offset vertically by the CEP, so that there are some photoelectron energies where the curves intersect and total constructive interference occurs.

When the CEP increases, as shown by the dotted phase curve, the intersections of the spectral phase curves change in energy and the positions of maximal constructive interference in the photoelectron spectrum move towards higher energy. In order to calculate the effect of the CEP and laser spectral phase, the 'weighted average' of multiphoton pathways can be approximated by an autoconvolution of the laser pulse. That is, neglecting the atomic phase and any resonances, the complex spectrum (amplitude and phase) of the N-photon absorption peak is the complex laser spectrum convoluted with itself N times. Numerical predictions for the case of the measured laser spectrum both as a transform-limited pulse and with a small chirp of 6 fs^2 are shown in figures 5(b) and (c), respectively. The positive chirp on the laser pulse makes the regions of maximal asymmetry move to higher energy with higher CEP. Now it is also clear why there are certain special photoelectron energies in figure 2 with no asymmetry in the photoelectron distribution, regardless of the CEP. These are places in the spectrum at the tops of the photoelectron peaks, where for the laser pulse bandwidth used, there are quantum paths with only one photon number that contributes significantly to the photoionization amplitude. With no contribution from opposite parity partial waves there is no interference, regardless of the CEP or chirp, as in panels (b) and (c) of figure 5. Thus, long pulses with narrow bandwidths would lead to zero asymmetry in the photoelectron spectrum even if the CEP were stabilized.

5. Chirp dependence

The preceding model confirms that some residual chirp remains on the pulse used for the experiment presented in figure 2. Figure 6(b) shows raw asymmetry data that indicate that after optimizing the laser pulse to reduce the chirp (at the cost of lower peak intensity and therefore the count rate), the linear CEP-dependence of the positions of maximum constructive and destructive interference disappears. Some CEP-dependent asymmetry variations persist, possibly a result of higher order spectral phase contributions from the laser pulse and spatial inhomogeneity in the detector dark count rate. Upon chirping the pulse by propagation through an extra 160 μm of fused silica, which imparts approximately 6.4 fs^2 of chirp, the linear pattern of figure 2(c) returns (figure 6(c)), qualitatively supporting the multiphoton model.

As a final note, we would like to point out that because ionization is a bound–free transition, the variation of the signal with CEP repeats every 2π radians. If a bound–bound transition like absorption were instead employed, the same multiphoton model would apply but the result would be a π-periodicity in the CEP measurement because in that case the parity selection rule only allows N-photon pathways to interfere with N+2-photon pathways. So, moving away from photoelectron spectroscopy to absorption or fluorescence measurements in atoms could enable single-pulse determination not of ϕ but rather of ϕ mod π.

6. Summary

When Xe atoms are ionized with 7 fs, CEP-stabilized laser pulses with peak intensity in the perturbative regime, the resulting photoelectron angular distributions are asymmetric along the polarization direction of the laser. The asymmetry depends on the energy of the photoelectron and the CEP of the laser pulse. The underlying mechanism for the observed asymmetry is quantum interference between equivalent pathways involving different numbers of photons. This mechanism is general to processes driven by perturbative laser pulses, including absorption, nonlinear optical frequency conversion and even coherent control. Indeed, the mechanism can be thought of as the basis for strong-field CEP effects as well, though in that regime more than just two quantum pathways lead to the same final state. This mechanism also opens the way to single-pulse determination of the CEP using perturbative fields as well as absolute phase spectroscopy of atoms for the investigation of scattering processes.

Acknowledgments

The authors wish to thank Lukas Gallmann, Jason Jones and Jun Ye for significant contributions to the experimental apparatus. The project is supported by a MURI program from the Air Force Office of Scientific Research, contract no. FA9550-04-1-0242. Portions of the laboratory were supported by the Director, Office Of Science, Office of Basic Energy Sciences, of the US Department of Energy under contract DE-AC02-05CH11231. TP acknowledges support of a Feodor Lynen Fellowship of the Alexander von Humboldt-Foundation. MJB and PMN are recently supported by a National Science Foundation Grant.

References

[1] Telle H R, Steinmeyer G, Dunlop A E, Stenger J, Sutter D H and Keller U 1999 *Appl. Phys.* B **69** 327
[2] Jones D J, Diddams S A, Ranka J K, Stentz A, Windeler R S, Hall J L and Cundiff S T 2000 *Science* **288** 635
[3] Keller U 2003 *Nature* **424** 831
[4] Zimmermann M, Gohle C, Holzwarth R, Udem T and Hänsch T 2004 *Opt. Lett.* **29** 310
[5] Baltuška A *et al* 2003 *Nature* **421** 611
[6] Pfeifer T, Jullien A, Abel M J, Nagel P M, Gallmann L, Neumark D M and Leone S R 2007 *Opt. Express* **15** 17120
[7] Paulus G G, Lindner F, Walther H, Baltuška A, Goulielmakis E, Lezius M and Krausz F 2003 *Phys. Rev. Lett.* **91** 253004
[8] Kling M F *et al* 2006 *Science* **312** 246
[9] Roos P A, Li X, Smith R P, Pipis J A, Fortier T M and Cundiff S T 2005 *Opt. Lett.* **30** 735
[10] Augst S, Meyerhofer D D, Strickland D and Chin S L 1991 *J. Opt. Soc. Am.* B **8** 858
[11] Ammosov M V, Delone N B and Krainov V P 1986 *Sov. Phys.—JETP* **64** 1191
[12] Saathoff G, Miaja-Avila L, Aeschlimann M, Murnane M M and Kapteyn H C 2008 *Phys. Rev.* A **77** 022903
[13] Yudin G L and Ivanov M Y 2001 *Phys. Rev.* A **64** 013409
[14] Loh Z H, Khalil M, Correa R E, Santra R, Buth C and Leone S R 2007 *Phys. Rev. Lett.* **98** 143601
[15] Adachi S and Kobayashi T 2005 *Phys. Rev. Lett.* **94** 153903
[16] Baltuška A, Fuji T and Kobayashi T 2002 *Phys. Rev. Lett.* **88** 133901
[17] Nakajima T and Watanabe S 2006 *Phys. Rev. Lett.* **96** 213001
[18] Roudnev V and Esry B D 2007 *Phys. Rev. Lett.* **99** 220406
[19] Kling M F, Rauschenberger J, Verhoef A J, Hasovic E, Uphues T, Milosevic D B, Muller H G and Vrakking M J J 2008 *New J. Phys.* **10** 025024
[20] Kienberger R *et al* 2004 *Nature* **427** 817
[21] Eppink A T J B and Parker D H 1997 *Rev. Sci. Instrum.* **68** 3477
[22] Parker D H and Eppink A T J B 1997 *J. Chem. Phys.* **107** 2357
[23] Drbinski V, Ossadtchi A, Mandelshtam V A and Reisler H 2002 *Rev. Sci. Instrum.* **73** 2634
[24] Wegener M 2005 *Extreme Nonlinear Optics* (Berlin: Springer)